ChemComm

RSC Publishing

COMMUNICATION

In situ atomic-scale visualization of oxide islanding during oxidation of Cu surfaces†

Cite this: *Chem. Commun.*, 2013, **49**, 10862

Received 1st September 2013, Accepted 2nd October 2013

DOI: 10.1039/c3cc46684a

www.rsc.org/chemcomm

Guangwen Zhou,*[a] Langli Luo,[a] Liang Li,[a] Jim Ciston,[b] Eric A. Stach,[c] Wissam A. Saidi[d] and Judith C. Yang[d]

Oxidation of Cu occurs *via* Cu_2O islanding on an oxide wetting layer at a critical thickness of two atomic layers. The transition from 2D wetting-layer growth to 3D oxide islanding is driven energetically arising from the Cu–Cu_2O interfacial interaction.

Fundamental understanding of metal oxidation has received extensive interest owing to its significant importance in many fields including high temperature corrosion, catalytic reactions, and thin film processing. Generally, the oxidation of metals involves hierarchical multiple length scales proceeding from oxygen surface chemisorption to oxide nucleation and growth and then to the formation of continuous oxide films. One of the most poorly understood and disputable phenomena in metal oxidation is its transient early stages, *i.e.*, how oxide films nucleate and start to grow, which are inaccessible by the traditional surface science and "bulk" materials science techniques.

Some simple pure metals and alloys have been studied for understanding the reaction mechanism in the transient oxidation stages.[1–11] These studies have shown that the early stages of metal oxidation typically involves oxide islanding, however, significant controversies exist regarding homogeneous or heterogeneous nucleation of oxide films. It was suggested that oxide nuclei should form at surface defect sites where threading dislocations or stacking faults intersect the surface (*i.e.*, a process controlled by heterogeneous island nucleation), but in most cases the evidence has been purely inferential.[2,3,5,12] Although oxide nuclei were observed to form at some dislocations, most nuclei did not show one-on-one correlation with dislocations and many dislocations have no oxide nuclei associated with them (*i.e.*, a process controlled by homogenous island nucleation).[1,13–15] A key challenge in resolving these controversies is the absence of direct observation of the structural transition in real space during oxidation due, in large part, to the inability of traditional experimental approaches to monitor the surface structure evolution and oxide formation with the desired spatial and temporal resolution.

In situ environmental transmission electron microscopy (TEM) has progressed dramatically in recent years. It can now allow for temperature-, time-, and pressure-resolved imaging of oxidation at the atomic scale with the development of aberration corrected microscopes coupled with differentially pumped environmental cells. Using dynamic real-time TEM observations of the nucleation and growth of Cu_2O islands during the oxidation of Cu, here we demonstrate that oxide islanding occurs homogeneously on an oxide wetting layer at a critical thickness of two atomic layers, which resembles the Stranski–Krastanov mechanism in heterogeneous thin film epitaxy.[16] This study offers the first experimental observation of the structure transition, on the atomic scale, of the nucleation and growth of 3D oxide islands and reveals that both heterogeneous and homogenous processes are involved leading to oxide islanding, where the heterogeneous process controls the nucleation of an oxide wetting layer at defect sites (*e.g.*, steps) on the metal surface while the homogeneous process controls the nucleation of 3D oxide islands on the oxide wetting layer driven by the metal–oxide interfacial strain.

The oxidation experiments were performed in a dedicated field-emission environmental TEM (FEI Titan 80-300) equipped with an objective-lens aberration corrector. The microscope has a spatial resolution of 0.8 Å in the high-resolution TEM mode at the elevated gas pressures local to the sample. Cu(001) single crystal thin films with ~500 Å thickness were grown on NaCl(001) by e-beam evaporation. The Cu films were removed from the substrate by floatation in deionized water, washed, and mounted on a TEM specimen holder. *In situ* TEM observation of the oxidation process was made in cross-sectional views by imaging along faceted Cu edges of empty holes created *in situ* inside the microscope by deliberately annealing the Cu films at ~600 °C under H_2 gas flow to generate tears and holes with faceted edges.

Fig. 1 shows a bright-field (BF) TEM image of the Cu(100) surface after oxidation at $T = 550$ °C and oxygen pressure $pO_2 = 1 \times 10^{-3}$ Torr.

[a] *Department of Mechanical Engineering, State University of New York at Binghamton, NY 13902, USA. E-mail: gzhou@binghamton.edu*

[b] *National Center for Electron Microscopy, Lawrence Berkeley National Laboratory, Berkeley, CA 94720, USA*

[c] *Center for Functional Nanomaterials, Brookhaven National Laboratory, Upton, NY 11973, USA*

[d] *Department of Chemical and Petroleum Engineering, University of Pittsburgh, Pittsburgh, PA 15261, USA*

† Electronic supplementary information (ESI) available: *In situ* TEM videos and DFT calculations of the total energies of Cu_2O thin films. See DOI: 10.1039/c3cc46684a

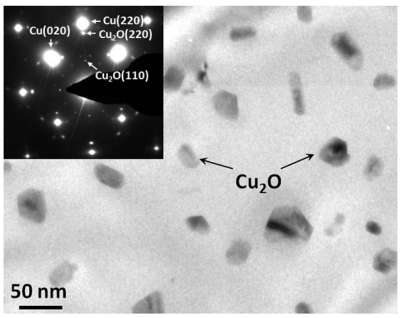

Fig. 1 BF-TEM image of a Cu(100) film oxidized at T = 550 °C and pO_2 = 1 × 10^{-3} Torr, showing oxide island formation. The inset shows a SAED pattern for the oxidized Cu film revealing the epitaxial growth of Cu_2O islands; additional reflections are due to double diffraction of electron beams by Cu and Cu_2O.

In the range of T and pO_2 employed in our study, the formation of the Cu_2O phase is thermodynamically favorable.[17,18] It shows clearly that the initial oxidation of the surface occurs *via* the formation of oxide islands rather than uniform, layer-by-layer growth of a continuous oxide film that is typically assumed by the classical theories of metal oxidation.[19,20] The TEM image suggests that oxide islands nucleate randomly across the surface, implying a homogeneous process of oxide islanding on the Cu surface. However, it should be noted that in this imaging mode it is not obvious if surface defects (*e.g.*, steps) are present, which may serve as the preferred sites for oxide formation. Meanwhile, it cannot be easily found from the planar imaging if the observed oxide islanding occurs on a wetting layer or just bare Cu surface. The inset shows a selected area electron diffraction (SAED) pattern obtained for the oxidized Cu film, which reveals that the oxide islands have a cube-on-cube epitaxy relationship with the Cu(100) substrate, where relative orientation between the Cu_2O islands and the Cu film is (001)Cu//(001)Cu_2O and [110]Cu//[110]Cu_2O.

Fig. 2 depicts *in situ* HRTEM images of a Cu(100) surface, seen edge-on under the oxidation conditions of pO_2 = 5 × 10^{-3} Torr and T = 350 °C. As seen in Fig. 2(a), some oxide has already developed on the surface from the oxidation before the *in situ* TEM movie was captured, where the lattice spacing matches well with the Cu_2O structure and can be used as a "fingerprint" for identifying the new oxides formed at later stages on the slightly lower left-hand side, where a two-atomic-layer-thick oxide wetting layer is visible. The top-left inset shows a zoom-in TEM image of the location where a Cu step is present at the Cu_2O–Cu interface in the region indicated by the dashed box. Due to their different lattice spacings, the Cu_2O(200) plane (dashed red line) is slightly higher than the Cu surface (solid red line), thereby forming a disconnection at the Cu step and giving rise to slight lattice distortion across the stepped region. This is illustrated in the corresponding structure model (top-right inset). It can be seen that two complete Cu_2O wetting layers have developed on the lower Cu terrace (*i.e.*, the left-hand side) while the third oxide layer still shows some discrete fuzzy features. The time sequence of TEM images in Fig. 2(b and c) shows the nucleation and growth of a 3D Cu_2O island on the Cu_2O wetting layer in the course of the oxidation. It is interesting to note that the 3D island nucleates on a flat surface region rather than atop the distorted Cu_2O layer above the buried Cu step, suggesting a homogenous process of oxide island nucleation on the wetting layer.

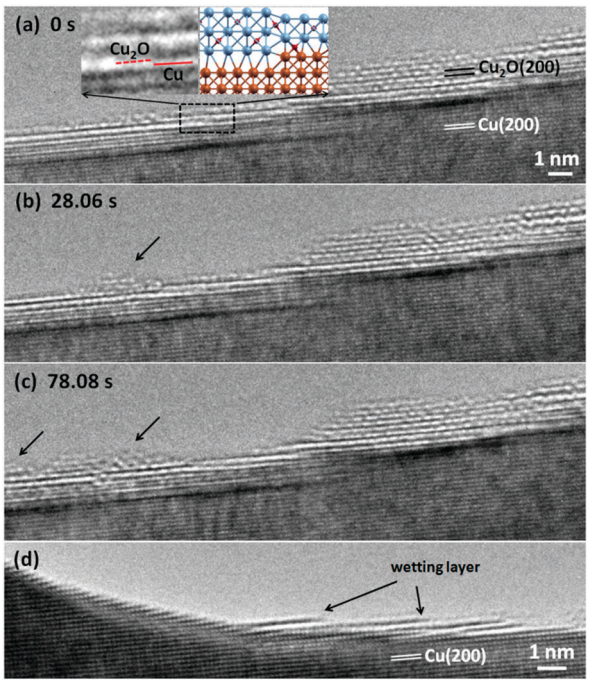

Fig. 2 (a–c) *In situ* TEM observations of the nucleation and growth of a Cu_2O island on the oxide wetting layer during oxidation of Cu(100) at 350 °C and pO_2 = 5 × 10^{-3} Torr (see *in situ* TEM movie S1 in the ESI†). Inset in (a) shows the formation of a disconnection at the buried Cu–Cu_2O interface due to the presence of an atomic Cu surface step. (d) TEM image revealing that the oxide wetting layers initiate at Cu surface steps.

However, it is noted that the nucleation of the oxide wetting layer occurs *via* a heterogeneous process at surface defects, as seen in Fig. 2(d), which shows that all the wetting layers can be traced back to Cu surface steps at the corner. The *in situ* TEM images also reveal that the thickness of the Cu_2O wetting layer is two atomic layers for the transition to the 3D Cu_2O island growth. Fig. 2(c) shows that a second Cu_2O island (part of it is out of the TEM view) forms adjacent to the existing island and their coalescence would result in a bigger island similar to the one seen on the right-hand terrace.

Fig. 3 presents a time sequence of *in situ* TEM images showing the oxide wetting layer thickness evolution leading to the nucleation of a 3D Cu_2O island during the oxidation at pO_2 = 5 × 10^{-3} Torr and T = 350 °C. In Fig. 3(a), a large Cu_2O island along with a Cu_2O wetting layer has already formed across the terrace before the *in situ* TEM movie was captured. The presence of atomic steps on the original Cu surface results in a slightly uneven surface morphology of the Cu_2O wetting layer. We focus on the wetting layer in the region having a flat surface as indicated by the black arrow in the figures. While the lattice fringe contrast of the wetting layer in this region appears to be slightly fuzzy, its thickness can be seen to be equivalent to three atomic layers by comparing with the well-resolved lattice fringe contrast in the adjacent large Cu_2O island. As seen in Fig. 3(a–c) and the *in situ* TEM movie (ESI†), the oxide wetting layer undergoes some fluctuation in height and eventually evolves into a stable 3D oxide island over time. Meanwhile, it can be noted that the thickness of the oxide wetting layer between the large existing island and the newly formed Cu_2O island changes gradually from the original three atomic layers to two atomic layers, where the atoms from the wetting layer are dislodged to the adjacent regions for oxide islanding.

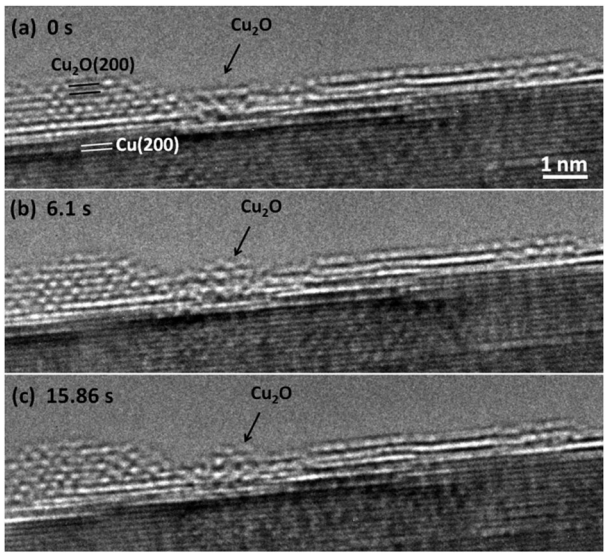

Fig. 3 (a–c) Time-resolved *in situ* TEM images showing the evolution of an initially three-atomic-layer-thick oxide wetting layer into a 3D Cu_2O island during the oxidation at 350 °C and $pO_2 = 5 \times 10^{-3}$ Torr (see *in situ* TEM movie S2 in the ESI†).

Such thickness reduction suggests that a continuous, three-atomic-layer-thick wetting layer is energetically unstable and transforms spontaneously to a more stable configuration by oxide islanding.

The natural lattice misfit between Cu and Cu_2O is 15.4% and this large misfit makes the formation of a coherent metal–oxide interface energetically unfavorable. We have previously shown that the epitaxial growth of Cu_2O thin films on Cu substrates results in a (5×6) coincidence site lattice (CSL) at the Cu_2O–Cu interface, in which 5 Cu spacings in the Cu_2O overlayer match 6 Cu spacings in the Cu substrate.[21,22] While the interfacial strain is significantly reduced to ~1.48% by adopting this CSL interface configuration, the associated strain energy still increases rapidly as the oxide wetting layer thickens. To relieve the strain, oxide island formation occurs on the oxide wetting layer, due to which the reduction in strain energy is greater than the concomitant cost of increased surface energy associated with creating the oxide island. The critical thickness of the wetting layer at which oxide islanding is initiated is two atomic layers, as seen in Fig. 2 and 3. To give further insight, we used density functional theory (DFT) to investigate the stability of the Cu_2O wetting layer for different thicknesses up to 4 Cu_2O layers. As shown in Fig. 4, in the optimized structure for the Cu–Cu_2O system with 4 Cu_2O layers, the interplanar spacings, from bottom to top, are 2.26 Å (the spacing between the Cu substrate and the bottom Cu_2O layer), 1.96 Å, 2.04 Å and 1.49 Å, respectively. Note that the bulk $Cu_2O(100)$ interplanar distance is 2.15 Å from our DFT calculation. The distance between the top and second Cu_2O layers is small compared to the bulk value, which can be attributed to the surface effect. Energetically, starting from a Cu slab with one Cu_2O layer on top, we found that it costs 2.7, 1.5 and 1.1 eV per Cu_2O to add 1, 2 and 3 additional layers. These DFT energies show that the interfacial energies are relatively large and the Cu–Cu_2O interface becomes increasingly unstable upon increasing the thickness of the wetting layer, and is likely to transform into an island as shown in the experiments. Further investigations to elucidate this transformation are needed but are beyond the present study.

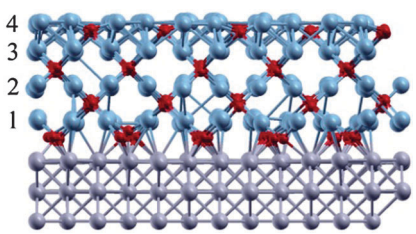

Fig. 4 Minimum-energy structure for a four-atomic-layer-thick Cu_2O wetting layer on Cu(001) with a (6×5) CSL at the Cu_2O–Cu interface. Our DFT calculations show that the Cu_2O–Cu interface becomes increasingly unstable when the wetting layer thickens (see ESI†).

In conclusion, we have demonstrated that oxide islanding occurs homogeneously on an oxide wetting layer nucleated from surface steps. The critical thickness of the oxide wetting layer at which oxide islanding is initiated is determined to be two atomic layers. We showed that such a transition to oxide islanding is driven energetically arising from the Cu_2O–Cu interfacial strain. Since oxide islanding is a typical step in metal oxidation, we expect broader applicability of our results for manipulating oxide growth morphology, properties, and long-term oxidation kinetics.

This work was supported by the U.S. Department of Energy, Office of Basic Energy Sciences, Division of Materials Sciences and Engineering, under Award No. DE-FG02-09ER46600. The research was carried out in part at the Center for Functional Nanomaterials, Brookhaven National Laboratory, which is supported by the U.S. Department of Energy, Office of Basic Energy Sciences, under Contract No. DE-AC02-98CH10886. This work used the Extreme Science and Engineering Discovery Environment (XSEDE), which is supported by National Science Foundation grant number OCI-105375.

Notes and references

1 K. R. Lawless, *Rep. Prog. Phys.*, 1974, **37**, 231–316.
2 P. H. Holloway and J. B. Hudson, *Surf. Sci.*, 1974, **43**, 123–140.
3 K. Heinemann, D. B. Rao and D. L. Douglass, *Oxid. Met.*, 1975, **9**, 379–400.
4 P. H. Holloway, *J. Vac. Sci. Technol.*, 1981, **18**, 653–659.
5 R. H. Milne and A. Howie, *Philos. Mag. A*, 1984, **49**, 665–682.
6 E. E. Hajcsar, P. R. Underhill and W. W. Smeltzer, *Langmuir*, 1995, **11**, 4862–4872.
7 J. C. Yang, D. Evan and L. Tropia, *Appl. Phys. Lett.*, 2002, **81**, 241–243.
8 G. W. Zhou and J. C. Yang, *J. Mater. Res.*, 2005, **20**, 1684–1694.
9 G. W. Zhou, J. A. Eastman, R. C. Birtcher, P. M. Baldo, J. E. Pearson, L. J. Thompson, L. Wang and J. C. Yang, *J. Appl. Phys.*, 2007, **101**, 033521.
10 K. Lahtonen, M. Hirsimaki, M. Lampimaki and M. Valden, *J. Chem. Phys.*, 2008, **129**, 124703.
11 G. W. Zhou, D. D. Fong, L. Wang, P. H. Fuoss, P. M. Baldo, L. J. Thompson and J. A. Eastman, *Phys. Rev. B*, 2009, **80**, 134106.
12 S. Zalkind, M. Polak and N. Shamir, *Surf. Sci.*, 2002, **513**, 501–510.
13 J. C. Yang, M. Yeadon, B. Kolasa and J. M. Gibson, *Scr. Mater.*, 1998, **38**, 1237–1241.
14 J. C. Yang, M. Yeadon, B. Kolasa and J. M. Gibson, *J. Electrochem. Soc.*, 1999, **146**, 2103–2106.
15 G. W. Zhou, L. Wang and J. C. Yang, *J. Appl. Phys.*, 2005, **97**, 063509.
16 E. Bauer, *Z. Kristallogr.*, 1958, **110**, 372–394.
17 X. Duan, O. Warschkow, A. Soon, B. Delley and C. Stampfl, *Phys. Rev. B*, 2010, **81**, 075430.
18 W. A. Saidi, M. Y. Lee, L. Li, G. W. Zhou and A. J. H. McGaughey, *Phys. Rev. B*, 2012, **86**, 245429.
19 C. Wagner, *Z. Phys. Chem., Abt. B*, 1933, **21**, 25–41.
20 N. Cabrera and N. F. Mott, *Rep. Prog. Phys.*, 1949, **12**, 163–184.
21 G. W. Zhou, *Appl. Phys. Lett.*, 2009, **94**, 233115.
22 G. W. Zhou, L. L. Luo, L. Li, J. Ciston, E. A. Stach and J. C. Yang, *Phys. Rev. Lett.*, 2012, **109**, 235502.

